PERGAMON

International Journal of Heat and Mass Transfer 45 (2002) 2373–2385

International Journal of HEAT and MASS TRANSFER

www.elsevier.com/locate/ijhmt

Numerical visualization of mass and heat transport for conjugate natural convection/heat conduction by streamline and heatline

Qi-Hong Deng, Guang-Fa Tang *

College of Civil Engineering, Hunan University, Changsha, Hunan 410082, People's Republic of China

Received 15 May 2001

Abstract

The method of numerical visualization of mass and heat transport for convective heat transfer by streamlines and heatlines are comprehensively studied. Functions are directly defined in terms of dimensionless governing equations or variables. Some basic characteristics of the functions are illustrated in detail, knowledge of which is essential to perceive the results and the philosophy of heat and fluid flow. The consistency of the formulations is especially addressed when dealing with conjugate convection/conduction problem. The functions/lines are unified for both fluid and solid regions, and the diffusion coefficients of the function equations are invariant. The method has been used to visualize the heat and fluid flow structures for natural convection in an air ($Pr = 0.71$) filled square cavity over a wide range of $Ra = 10^3 - 10^6$, and those for conjugate natural convection/heat conduction problem where the conduction effect of solid body on heat transfer is investigated. As to exhibiting the nature of convective heat transfer, streamlines and heatlines provide a more practical and efficient means to visualize the results than the customary ways.

1. Introduction

Numerical modeling of convective heat transfer problem has been an area of great interest in the recent years due to its wide application in engineering. Compared to experimental method, numerical analysis may provide a more direct way on how to enhance/reduce heat transfer effectively so as to improve the performance or to optimize the structure of thermal device. However, numerical results for convective heat transfer are now basically presented by distributions of primitive variables such as velocity and temperature, which describe the state of the system locally but not its physically associated structure. In essence, the process of convective heat transfer is a combination of both mass and heat transport, numerical visualization of the two transport processes is therefore a more direct approach to investigate the structure or characteristics of the heat and fluid flow with insight to the philosophy of convective heat transfer.

Streamfunction and streamlines are very efficient and being widely used tools to visualize momentum transport of fluid flow. To visualize the transfer of heat by fluid flow, an energy analog concept, heatfunction and heatlines, was first introduced by Kimura and Bejan [1] in 1983, which provides a better visualization technique as compared to the traditional isotherm approach. The method has been adopted and extended in several ways in the following literature [2–9]. But these heatline applications are basically limited to natural convection with simple boundary conditions except for the laminar boundary layer flow [6]. It is worth noting that Costa [8,9] gave a unified viewpoint in both physical and numerical aspects on treatment of the functions and lines for visualizing two-dimensional transport problem, which would be helpful to guide the applications henceforth. However, as Costa dealt with conjugate transfer problem, the assertion of variable diffusion coefficient and the practice of harmonic mean for functions

* Corresponding author. Tel.: +86-731-882-2760; fax: +86-731-882-1342.

E-mail address: gftang@mail.hunu.edu.cn (G.-F. Tang).

0017-9310/02/$ - see front matter
PII: S0017-9310(01)00316-7

Nomenclature

A	area
c_p	isobaric specific heat
g	gravitational acceleration
H	dimensionless heat function
J	transport flux vector
k	thermal conductivity
L	length of enclosure
$\overline{Nu}$	average Nusselt number
p	pressure
P	dimensionless pressure ($P = (p/\rho)(L/\alpha)^2$)
Pr	Prandtl number ($Pr = v/\alpha$)
Ra	Rayleigh number ($Ra = g\beta\Delta TL^3/v\alpha$)
s	segment
S	source term
T	temperature
u, v	Cartesian velocities
U, V	dimensionless Cartesian velocities ($(U, V) = (u, v)L/\alpha$)
x, y	Cartesian coordinates
X, Y	dimensionless Cartesian coordinates ($(X, Y) = (x, y)/L$)

Greek symbols

α	fluid thermal diffusivity
β	fluid thermal expansion coefficient
v	fluid kinematic viscosity
ρ	fluid density
θ	dimensionless temperature ($\theta = (T - T_c)/\Delta T$)
ΔT	temperature difference between hot and cold walls ($\Delta T = T_h - T_c$)
Γ	general diffusion coefficient
ϕ	general variable
Φ	general function related to ϕ
ψ	dimensionless streamfunction

Subscripts

c	cold
f	fluid
h	hot
max	maximum
min	minimum
s	solid

Superscripts

$*$	thermo-physical property ratio

are not correct because the constraints of flux balance at fluid–solid interface cannot be satisfied in this case as it will be detailed in the context.

In spite of its usefulness, application of the heatline visualization technique is limited. One main reason is that the basic characteristics exhibited cannot be measured by experiment as well. The method needs to be assessed by application to more complex problems. This motivates the present work.

To evaluate the value of the method for using streamlines and heatlines to visualize the mass and heat transport phenomena for convective heat transfer, the current research is to extend its application to more complex systems: conjugate problem between natural convection and heat conduction, and mixed convection problem combined the buoyancy driven and the forced flows. The former is considered in this paper, while the latter will be treated in the next paper. Firstly, the functions (including streamfunction and heatfunction) are defined in terms of dimensionless governing equations or variables, which provide a more general and straightforward visualization means than the customary definitions based on dimensional variables. Secondly, some important characteristics of the functions and their corresponding contour lines are systematically analyzed to further understand the principle of the convective heat transfer. Finally, consistency of the diffusion coefficient of the functions for conjugate problem, was established, which makes it easier to visualize the results. The objective of the present work is to visualize the characteristics of the heat transfer and fluid flow for natural convection in an air-filled square cavity over a wide range of Raleigh number ($Ra = 10^3$–10^6) by means of streamlines and heatlines, and also to examine the effects of conducting body centered in the cavity on heat transfer across the cavity.

2. Analysis and formulation

The conjugate heat transfer problem considered in this paper is schematically shown in Fig. 1. It is a closed square cavity with sides of length L, within which a conducting body, with sides of length $L/2$ and thermal conductivity k_s, is centered. The left and right side walls are isothermal at temperatures of T_h and T_c, respectively, whereas the bottom and top surfaces are thermally insulated. The gravitational acceleration acts parallel to the isothermal walls. It is assumed here the fluid properties being constant, except for the density in buoyancy term following the Boussinesq approximation. Be aware that when the size of the solid body decreases to zero, or without the solid conducting body, the conjugate heat transfer problem would turn to pure natural convection.

A two-dimensional, steady state, incompressible laminar flow model is considered in the present study. The non-dimensional conservative governing equations are written in general form as follows:

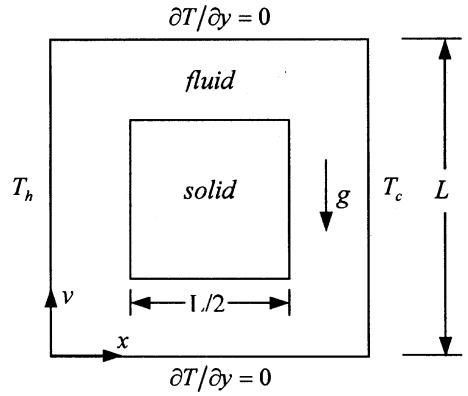

Fig. 1. Schematic of square cavity with centered solid body.

Continuity

$$\frac{\partial U}{\partial X}+\frac{\partial V}{\partial Y}=0. \tag{1}$$

X-Momentum

$$\frac{\partial}{\partial X}(UU)+\frac{\partial}{\partial Y}(VU)=v^{*}Pr\left(\frac{\partial^{2}U}{\partial X^{2}}+\frac{\partial^{2}U}{\partial Y^{2}}\right)-\frac{\partial P}{\partial X}. \tag{2}$$

Y-Momentum

$$\frac{\partial}{\partial X}(UV)+\frac{\partial}{\partial Y}(VV)=v^{*}Pr\left(\frac{\partial^{2}V}{\partial X^{2}}+\frac{\partial^{2}V}{\partial Y^{2}}\right)-\frac{\partial P}{\partial Y}+RaPr\theta. \tag{3}$$

Energy

$$\rho^{*}c_{\mathrm{p}}^{*}\left[\frac{\partial}{\partial X}(U\theta)+\frac{\partial}{\partial Y}(V\theta)\right]=k^{*}\left(\frac{\partial^{2}\theta}{\partial X^{2}}+\frac{\partial^{2}\theta}{\partial Y^{2}}\right). \tag{4}$$

The non-dimensional parameters are defined in terms of fluid properties as

$$(X,Y)=(x,y)/L,\quad (U,V)=(u,v)L/\alpha,$$
$$P=(p/\rho)(L/\alpha)^{2},\quad \theta=(T-T_{\mathrm{c}})/\Delta T,$$
$$Pr=v/\alpha,\quad Ra=g\beta\Delta TL^{3}/v\alpha.$$

In order to distinguish the solid from the fluid, we introduce three relative parameters v^{*}, k^{*} and $\rho^{*}c_{\mathrm{p}}^{*}$ referred to thermo-physical property ratios of solid to fluid; they are all unity in fluid but equal to infinity (in fact, a very high value), $K_{\mathrm{s}}/K_{\mathrm{f}}$, and unity, in solid zone, respectively. Note that when the velocities approach zero in the solid zone, the solution of energy equation (4) is independent of the value of $\rho^{*}c_{\mathrm{p}}^{*}$. For simplicity, we assign, $\rho^{*}c_{\mathrm{p}}^{*}=1$ in the context, so as to obtain an analog form between energy and momentum equations.

It should be pointed out that a high value of the relative kinematic viscosity v^{*} in solid region would make the velocity components negligibly small by solving momentum equations, then the continuity equation is automatically satisfied thereby. Correspondingly, the energy equation is reduced to heat conduction equation for the solid body, because its convection terms vanish. The state of art in the coupled convection and conduction analysis lies in that the same set of conservative equations (1)–(4) is simultaneously solved over the entire domain including both fluid and solid regions.

Eqs. (1)–(4) can be numerically solved by SIMPLE algorithm detailed in [10]. In order to improve numerical accuracy, the third-order deferred correction QUICK scheme [11] and second-order central difference are, respectively, employed for the convection and the diffusion terms. To solve the conjugate problem, the grid layout is such that the fluid–solid (F–S) interface forms a control volume face for the neighboring grid points. The abrupt changes of thermal conductivities at the interface between the fluid and solid regions are handled by harmonic mean formulation [10]. In this way, the energy balance, i.e., continuity of temperature and heat flux, across the interface is automatically well established. The global solution procedure facilitates the code programming, making it easier to solve the conjugate heat transfer problem, regardless of increasing requirement of computational storage and time. This is evident further for the complex problems involving multiple F–S interfaces, as the considered case with four F–S interfaces inside the cavity.

Boundary conditions of the entire computational domain for velocity and temperature in non-dimensional form are taken as follows:

$$\text{At } X=0:\quad U=V=0,\quad \theta=1, \tag{5}$$

$$\text{At } X=1:\quad U=V=0,\quad \theta=0, \tag{6}$$

$$\text{At } Y=0 \quad \text{and} \quad Y=1:\quad U=V=0,\quad \partial\theta/\partial Y=0. \tag{7}$$

The whole heat transfer characteristics across the cavity are described by the average Nusselt number, which is based on the enclosure length and the thermal conductivity of the fluid. For the hot wall, it is expressed by

$$\overline{Nu}_{\mathrm{h}}=-\int_{0}^{1}\left.\frac{\partial\theta}{\partial X}\right|_{X=0}\mathrm{d}Y, \tag{8}$$

and for the cold wall, by

$$\overline{Nu}_{\mathrm{c}}=-\int_{0}^{1}\left.\frac{\partial\theta}{\partial X}\right|_{X=1}\mathrm{d}Y. \tag{9}$$

By conservation of energy across the enclosure, the average Nusselt numbers at the hot and cold walls should

be equal, i.e., $\overline{Nu_h} = \overline{Nu_c}$, because the top and bottom surfaces are adiabatic.

Now, according to Bejan [1] and Costa [9], the definitions of streamfunction and heatfunction can be physically unified to satisfy automatically the continuity and the net energy equations, respectively. In this paper, the functions are defined in terms of dimensionless governing equations. As will be worked out, the derivation is more general and straightforward.

The general conservative dimensionless transport equation of continuity and energy equations without source term can thus be expressed in total flux form (consists of convection and diffusion) as

$$\frac{\partial}{\partial X}\left(U\phi - \Gamma_\phi \frac{\partial \phi}{\partial X}\right) + \frac{\partial}{\partial Y}\left(V\phi - \Gamma_\phi \frac{\partial \phi}{\partial Y}\right) = 0, \tag{10}$$

where the meanings of the dependent variable ϕ and its diffusion coefficient Γ_ϕ are listed in Table 1. The ϕ flux components in X and Y directions are, respectively, identified as

$$J_{\phi,X} = U\phi - \Gamma_\phi \frac{\partial \phi}{\partial X}, \quad J_{\phi,Y} = V\phi - \Gamma_\phi \frac{\partial \phi}{\partial Y}. \tag{11}$$

We define a new function $\Phi(X, Y)$ in such a way that a constant Φ line is parallel to the flux flow J_ϕ, or, the flux across the constant line is zero, which can be expressed in mathematical manner as

$$\mathrm{d}\Phi = J_\phi \times \mathrm{d}s = -J_{\phi,Y}\mathrm{d}X + J_{\phi,X}\mathrm{d}Y = 0, \tag{12}$$

where the symbol ($\times$) is the cross product, and ds is differential of the line. Expanding the total differential equation (12) yields the definition of the general function $\Phi(X, Y)$ in differential form as follows:

$$\begin{aligned} -\frac{\partial \Phi}{\partial X} &= J_{\phi,Y} = V\phi - \Gamma_\phi \frac{\partial \phi}{\partial Y}, \\ \frac{\partial \Phi}{\partial Y} &= J_{\phi,X} = U\phi - \Gamma_\phi \frac{\partial \phi}{\partial X}. \end{aligned} \tag{13}$$

Note that the definition of $\Phi(X, Y)$ satisfies Eq. (10) identically, that is: when ϕ is unity, Eq. (10) is continuity equation, and the corresponding definition in Eq. (13) is streamfunction as usual; when ϕ represents the dimensionless temperature, Eq. (10) becomes energy equation, and Eq. (13) is then the definition of heatfunction. This relationship between the general function Φ and the variable ϕ is also tabulated in Table 1.

According to the definition mentioned above, one can easily draw an important property of the functions. Given that the flux flows through two arbitrarily constant Φ lines as shown in Fig. 2, because no flux crosses the constant lines and also no source exists between the lines, the flux entering the area A_1 must be equal to that leaving to area A_2, namely

$$J_{\phi,1} \cdot A_1 = J_{\phi,2} \cdot A_2, \tag{14}$$

where $J_{\phi,1}$ and $J_{\phi,2}$, respectively, refer to the mean fluxes across the area A_1 and A_2.

Some basic characteristics of streamlines and heatlines, based on the definition and the property of the proposed functions, Eqs. (13),(14), can be worked out as follows:

1. For the definition of function is in terms of its first order derivatives, what is of importance or meanings are the differences between Φ's values but not the values themselves. That is, difference in value of streamlines denotes flow flux between the streamlines, and that of heatlines expresses the flux of heat between heatlines.
2. As the flux cannot approach infinity, the area between the lines cannot be zero, which means that a constant Φ line either starts and stops at boundaries or circulates as vortices.
3. From Eq. (14), the flux run through the area is inversely proportional to the size of area, the smaller the distance between Φ lines, or the denser the Φ lines, the larger the flux.
4. In the solid zone, i.e., $U = V = 0$, the streamfunction would keep constant as indicated by Eq. (13), then the solid surfaces would be a streamline, and no streamlines exist in the solid. Meanwhile, the heatfunction formulation would reduce to heat-flux function corresponding to heat conduction in solid zone, and therefore, heatline visualizing the convective heat transfer is the counterpart or the generalization of heat flux line used in conduction.
5. As shown by definition, streamfunction represents the strength of convection, while heatfunction ex-

Table 1
General variable (ϕ) and diffusion coefficients (Γ_ϕ) of the governing equations and their corresponding Φ functions

Physical principle	ϕ	Γ_ϕ	Φ	Φ Contour plots
Mass conservation	1	0	ψ	Streamlines
Energy conservation	θ	k^*	H	Heatlines

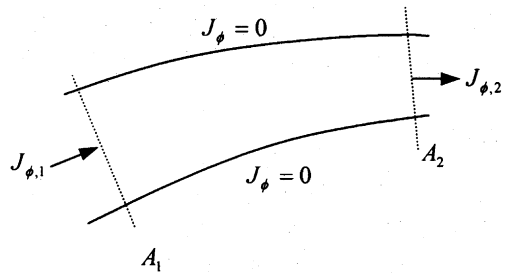

Fig. 2. Flux passing through two constant Φ lines.

presses the relative magnitude of strength between convection and diffusion or conduction.

At the fluid–solid interface, the balance constraints will be

$$U = V = 0, \tag{15}$$

$$\left.\frac{\partial\theta}{\partial X}\right|_{\mathrm{f}} = k^{*}\left.\frac{\partial\theta}{\partial X}\right|_{\mathrm{s}}, \quad \left.\frac{\partial\theta}{\partial Y}\right|_{\mathrm{f}} = k^{*}\left.\frac{\partial\theta}{\partial Y}\right|_{\mathrm{s}}. \tag{16}$$

Substituting Eqs. (15),(16) into Eq. (13), yields the relations of streamfunction and heatfunction at the fluid–solid interface

$$\left.\frac{\partial\psi}{\partial X}\right|_{\mathrm{f}} = \left.\frac{\partial\psi}{\partial X}\right|_{\mathrm{s}}, \quad \left.\frac{\partial\psi}{\partial Y}\right|_{\mathrm{f}} = \left.\frac{\partial\psi}{\partial Y}\right|_{\mathrm{s}}, \tag{17}$$

$$\left.\frac{\partial H}{\partial X}\right|_{\mathrm{f}} = \left.\frac{\partial H}{\partial X}\right|_{\mathrm{s}}, \quad \left.\frac{\partial H}{\partial Y}\right|_{\mathrm{f}} = \left.\frac{\partial H}{\partial Y}\right|_{\mathrm{s}}. \tag{18}$$

It is evident that the diffusion coefficients for energy equation θ change from 1 in fluid region to k^{*} in solid region, while the coefficients for heatfunction $H$are invariant, both equal to unity. In fact, they reflect the identical interface constraint of energy balance, i.e., continuity of heat flux. However, Costa [8,9] took the diffusion coefficients at the interface for heatfunction as being variable, ranging from 1 on fluid side to $1/k^{*}$ on solid side, which is not true, because the energy balance constraints at interface, Eq. (16), cannot be ensured so. Eliminating the gradient terms in Eq. (13) by cross partial differentiation, yields

$$0 = \frac{\partial^2\Phi}{\partial X^2} + \frac{\partial^2\Phi}{\partial Y^2} + \frac{\partial}{\partial X}(V\phi) - \frac{\partial}{\partial Y}(U\phi). \tag{19}$$

This is a conduction-type equation, with source term if the fluid flow subsists or without source term if the fluid flow subsides. An important aspect is that the Φ fields can be solved by the same numerical procedures and routines as those used for the primitive variable ϕ by introducing zero convection coefficients, as pointed out by Costa [9]. Since the diffusion coefficients of Eq. (19) are consistent for both fluid and solid regions, the harmonic mean procedure is not needed to calculate the coefficients at F–S interface and the values of function Φ at interface are not needed for drawing contour plots.

For solving Eq. (19), we now focus on the boundary conditions of Φ fields. Due to the relativity of Φ value, one should select a reference point on the boundary where its value is assumed to be zero. Then the Φ values over the boundaries including the reference point can be obtained by integrating the derivatives presented in Eq. (13) through the directions of boundaries. Hence, the boundary conditions of streamfunction and heatfunction for the considered conjugate heat transfer problem shown in Fig. 1 can be defined below:

$$\text{First set } \psi(0,0) = H(0,0) = 0, \tag{20}$$

$$\text{At } Y = 0: \quad H(X,0) = H(0,0) - \int_0^X \left(V\theta - \frac{\partial\theta}{\partial Y}\right)\mathrm{d}X = 0, \tag{21}$$

$$\text{At } X = 0: \quad H(0,Y) = H(0,0) + \int_0^Y \left(U\theta - \frac{\partial\theta}{\partial X}\right)\mathrm{d}Y = -\int_0^Y \frac{\partial\theta}{\partial X}\mathrm{d}Y, \tag{22}$$

$$\text{At } X = 1: \quad H(1,Y) = H(1,0) + \int_0^Y \left(U\theta - \frac{\partial\theta}{\partial X}\right)\mathrm{d}Y = -\int_0^Y \frac{\partial\theta}{\partial X}\mathrm{d}Y, \tag{23}$$

$$\text{At } Y = 1: \quad H(X,1) = H(0,1) - \int_0^X \left(V\theta - \frac{\partial\theta}{\partial Y}\right)\mathrm{d}X = -\int_0^1 \left.\frac{\partial\theta}{\partial X}\right|_{X=0}\mathrm{d}Y = \overline{Nu}_{\mathrm{h}}. \tag{24}$$

Noting that there is no flow flux through enclosure, the boundary conditions of streamfunction are all zeroes by integrating the streamfunction definition, Eq. (13), along boundaries.

The averaged Nusselt number would be provided directly by the heatline boundary conditions, and thus, the total heat transfer across the cavity can be graphically shown by the heatlines.

3. Results and discussion

To validate the method of present solution, the predicted values of pure natural convection in a air-filled square cavity, as schematically shown in Fig. 1 but without centered solid body, are compared with the benchmark results [12]. As shown in Table 2, the maximum values of absolute streamfunction and the average Nusselt numbers agree to within 2.5% and 1%, respectively, with the benchmark solutions for Rayleigh numbers up to 10^6. This confirms the accuracy of the present method.

Then, we used the method to investigate the heat transfer and flow structures of the natural convection in

Table 2
Comparisons of the present results with benchmark resolution for natural convection in square cavity in presence of air ($Pr = 0.71$)

Ra	Present		Benchmark [8]	
	$\lvert\psi\rvert_{\max}$	$\overline{Nu}$	$\lvert\psi\rvert_{\max}$	$\overline{Nu}$
10^3	1.17	1.118	–	1.118
10^4	5.04	2.254	–	2.243
10^5	9.50	4.557	9.612	4.519
10^6	16.32	8.826	16.750	8.800

an air-filled square cavity with a centered solid body with relative thermal conductivity of $k^* = 5$, as shown in Fig. 1. According to governing equations (1)–(4), the solutions will be determined only by the Rayleigh number, *Ra*, whose effect on the convective heat transfer is studied in the following.

3.1. Natural convection

Results of natural convection for Rayleigh numbers $Ra = 10^3$–10^6 are, respectively, shown in Figs. 3–6 by means of streamlines, heatlines, velocity profiles and isotherms. The streamfunction, ψ, and heatfunction, *H*, described vividly the transport path of mass and heat, while the velocity profiles and isothermals are in terms of primitive variables (V, θ) customary.

First of all, it should be noticed that there are some common interesting characteristics among the streamlines and the heatlines for all cases generalized as follows.

As mentioned before, the constant Φ lines either start and stop at boundaries or circulate as vortices. Since

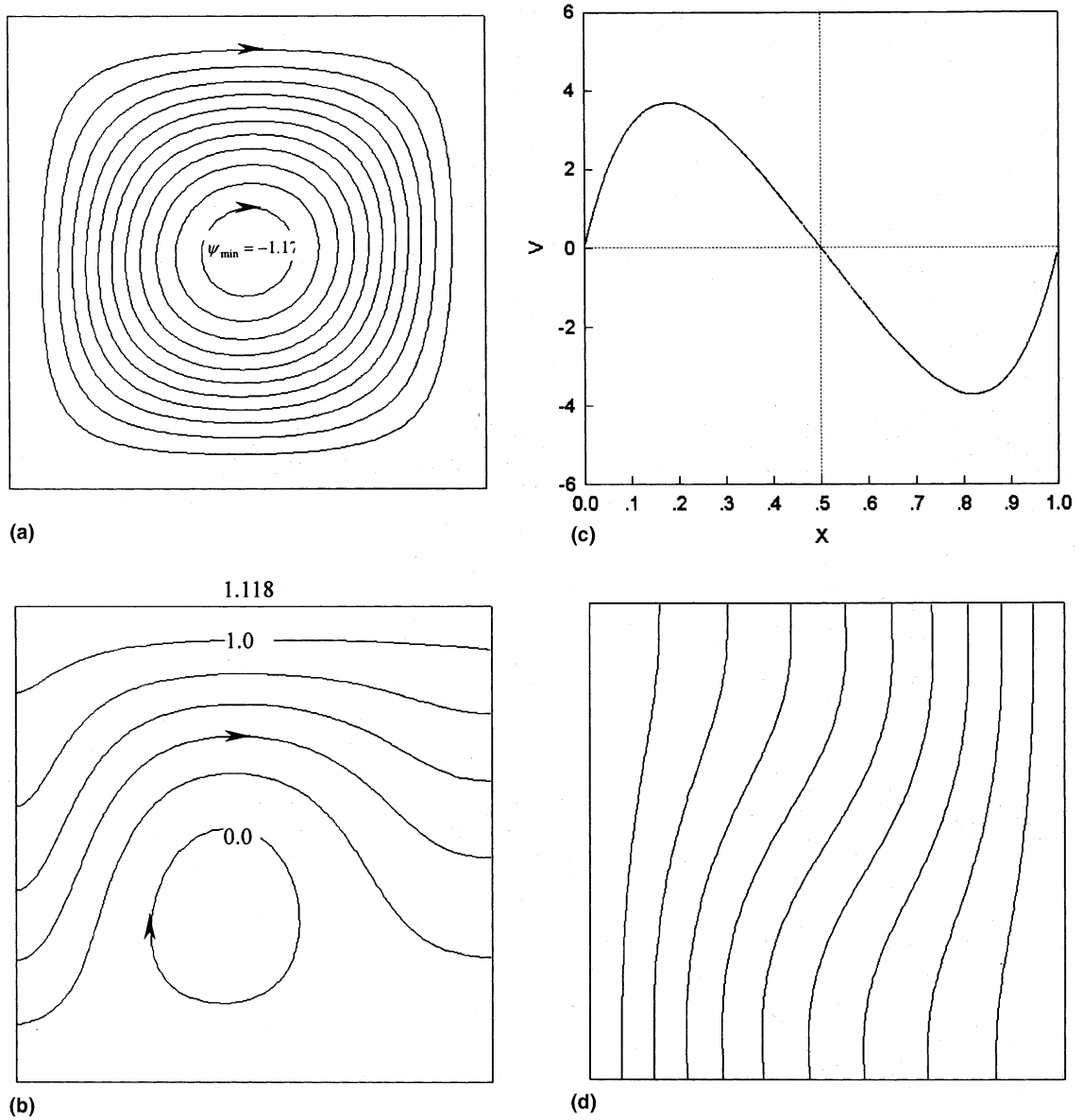

Fig. 3. Results of natural convection at $Ra = 10^3$ in an air-filled square cavity: (a) Streamlines whose incremental step is 0.1; (b) heatlines whose incremental step is 0.2; (c) velocity – *V* profiles along the horizontal centerline *X*; (d) isothermal whose incremental step is 0.1.

there is no mass or fluid exchange between the system of the cavity and its environment, the streamlines are all circulated as vortices. However, heat is absorbed from the left hot wall and released through the right cold wall. Therefore, some heatlines start from the hot wall and stop at the cold wall, which are responsible for the heat exchange between the system and the environment. Noting that, the function values are of relativity, their signs are dependent on the chosen reference point of zero value. For the boundary conditions of the functions as specified by Eqs. (20)–(24), the positive values of lines (either streamline or heatline) refer to the system mass or heat transfer. On the contrary, the negative value implies the inner transfer of the system. Therefore, all the values of streamlines are negative, but the values of heatlines are different, which is positive for those end-to-end at walls and negative for those eddies. In fact, both of the two horizontal adiabatic walls will be heatlines accordingly.

The heatline of maximum value, provides directly the value of the average Nusselt number, which reflects the total amount of the heat transfer across the cavity.

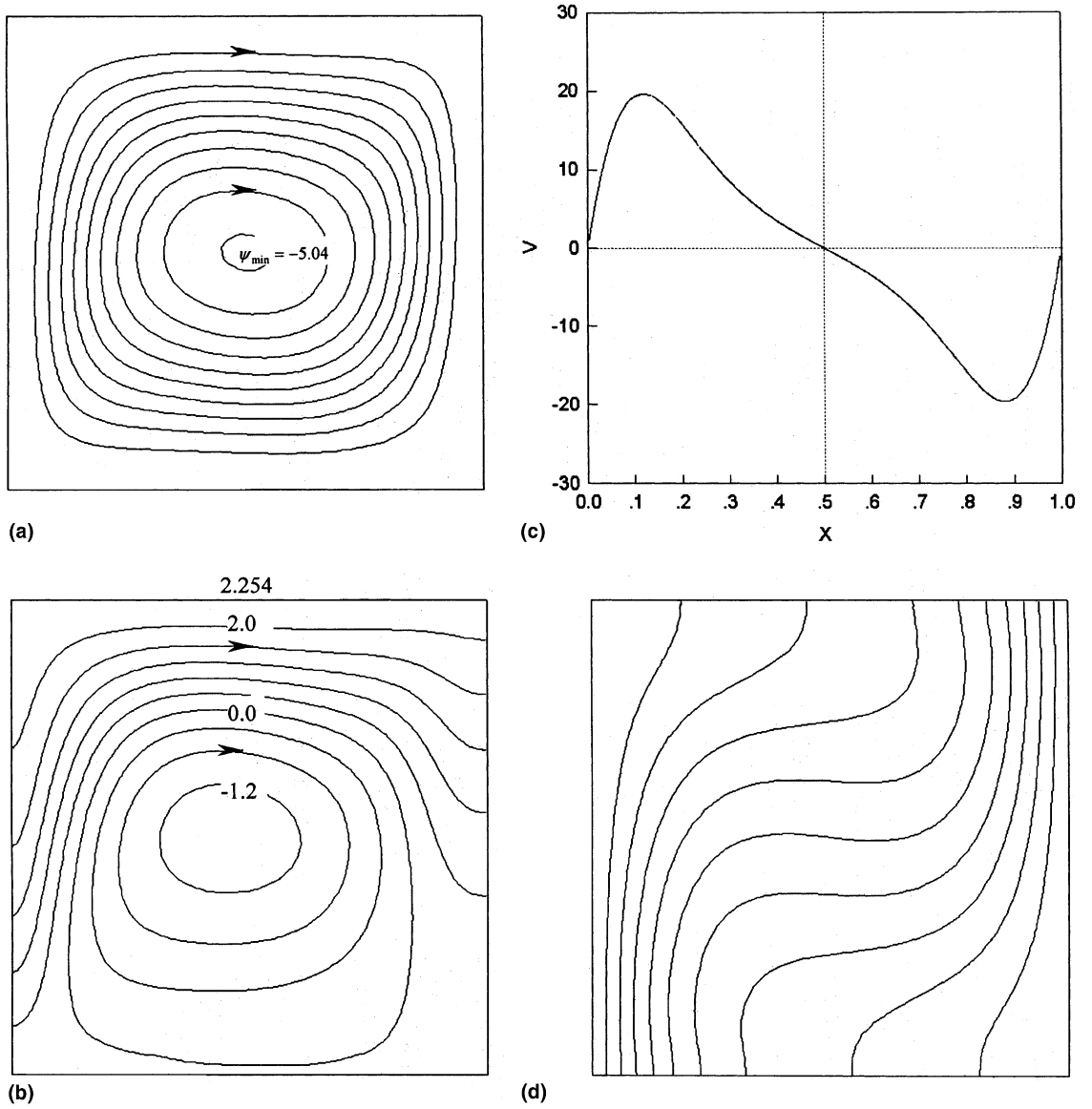

Fig. 4. Results of natural convection at $Ra = 10^4$ in an air-filled square cavity: (a) Streamlines whose incremental step is 0.5; (b) heatlines whose incremental step is 0.4; (c) velocity – V profiles along the horizontal centerline X; (d) isothermal whose incremental step is 0.1.

The heatlines crossing the hot wall are more crowded near the bottom side than those near the topside. This heatline pattern visualizes the non-uniform distribution of the heat flux over the walls, and is supported also by isotherms, i.e. the larger the heat flux, the sharper the isotherms changes.

At low Rayleigh number, $Ra = 10^3$, as shown in Fig. 3, the streamlines are of clockwise unicellular flow structure, and their relative low values such as $\psi_{\min} = -1.17$ indicate that the convection is very weak. Accordingly, the heat transfer across the cavity is mainly dominated by conduction, and thereby the heatlines and the isotherms both exhibit pseudo-conduction structure. The maximum value of heatlines, or average Nusselt number, 1.118, indicates that the heat transfer across the cavity is small in this case because of the low thermal conductivity of air.

Fig. 4 illustrates the results at Rayleigh number $Ra = 10^4$. The convection is strengthened, as indicated by the minimum value of streamlines, $\psi_{\min} = -5.04$. The

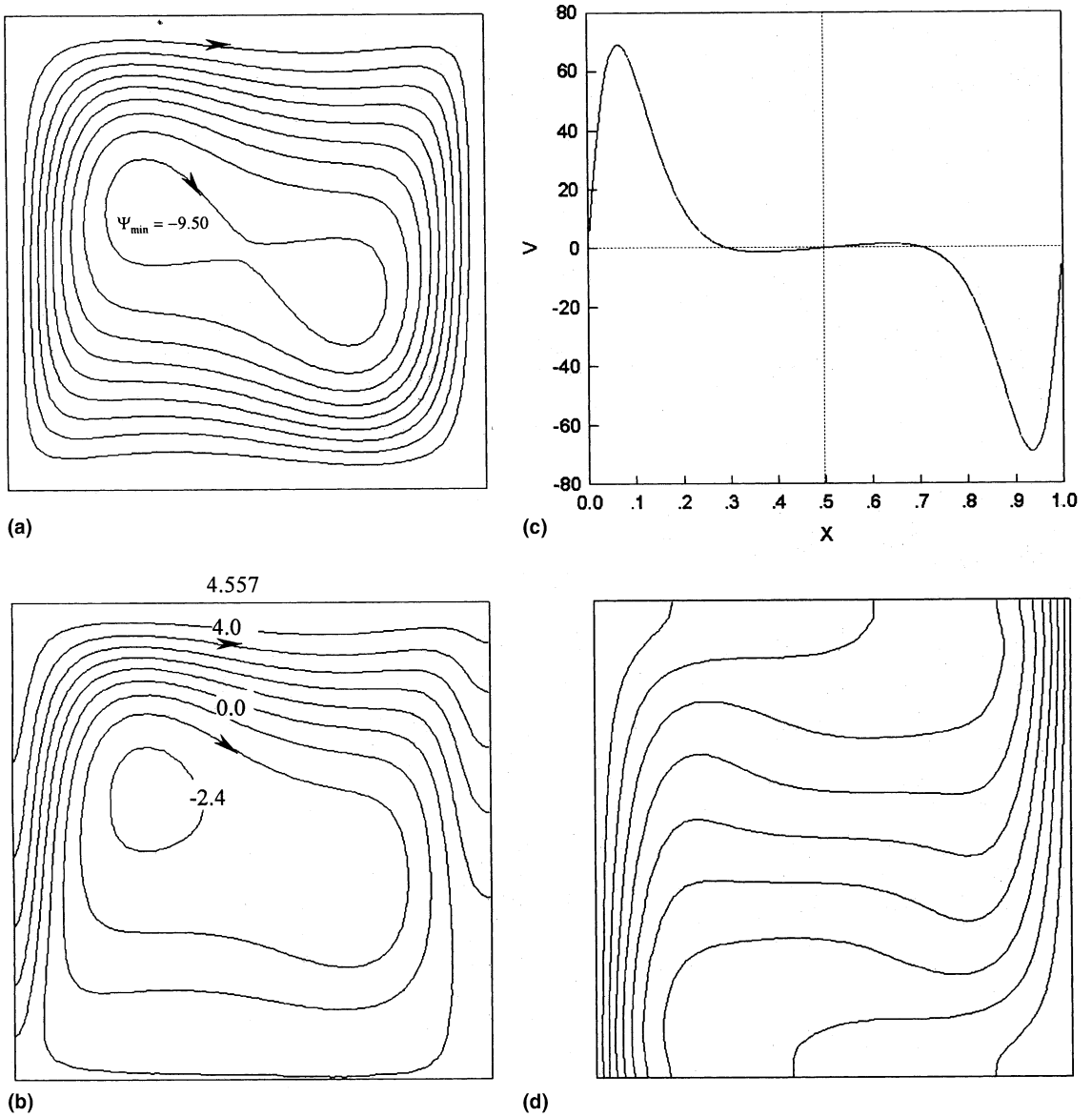

Fig. 5. Results of natural convection at $Ra = 10^5$ in an air-filled square cavity: (a) Streamlines whose incremental step is 0.1; (b) heatlines whose incremental step is 0.8; (c) velocity – V profiles along the horizontal centerline X; (d) isothermal whose incremental step is 0.1.

non-uniform distribution of streamlines implies that the flow flux or convection is stronger in the outer region than that in the center region. The effect of growing convection is more pronounced in heatlines and isotherms. It is interesting to find that the width of the heat boundary layers is approximately the distance between the position of velocity extremes and the isothermal walls layers, where heat is absorbed or released rapidly, and thus the temperature changes abruptly as exhibited by isotherms. Moreover, since the system heat transfer occurs in the upper part of the cavity, the temperature stratification is gradually formed. As a result, the air through the upper part is hotter than the lower part, which leads to the temperature highest in the top left corner. It should be emphasized that the conduction is now still an important heat transport mechanism compared with convection, for there are a quantity of heatlines circulate in the core. The maximum value of heatline, 2.254, indicates that the heat transfer across the cavity is enhanced by the increasing convection.

As the Rayleigh number further increased up to 10^5, shown in Fig. 5, there are distinct characteristics in the

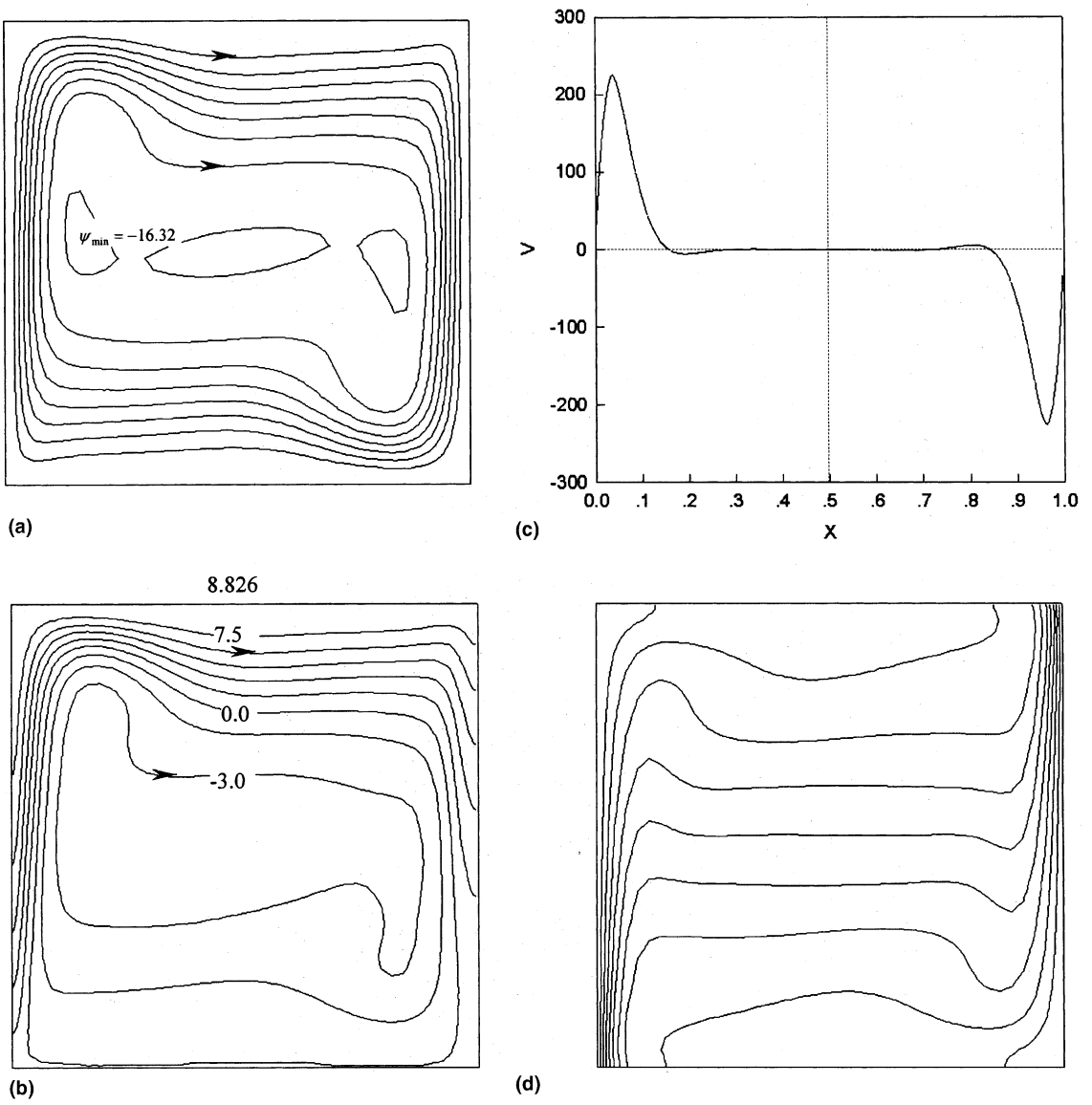

Fig. 6. Results of natural convection at $Ra = 10^6$ in an air-filled square cavity: (a) Streamlines whose incremental step is 2.0; (b) heatlines whose incremental step is 1.5; (c) velocity – V profiles along the horizontal centerline X; (d) isothermal whose incremental step is 0.1.

streamlines: it is of bicellular flow structure, and the convection is much increased as indicated by $\psi_{\min} = -9.50$. The non-uniform distribution of streamlines implies that the convection is strong in the outer region but weak in the core where the fluid is almost stagnant. These characteristics interpret that, convection becomes a dominant mechanism to transport the heat, which is more clearly depicted by heatlines. The rareness of heatlines in the half center region indicates that the role of conduction being markedly weakened in the process of heat transfer. The maximum value of heatlines, or average Nusselt number, 4.557, indicates that the heat transfer is further strengthened.

When Rayleigh number rises up to 10^6, as shown in Fig. 6, the convection is amplified again and has played a fully dominant role in the process of heat transfer. As expected, the streamlines are basically clustering in the thin outer region and rare in the inner region. The thermal boundary conditions have much influence on fluid in the outer region but little in the core where the air remains nearly stationary. This characteristic is confirmed by heatlines where both the thickness of the vertical boundary layers and the width of the horizontal channel decrease further. Accordingly, the heat transfer is enhanced up to the highest level of $\overline{Nu} = 8.826$.

3.2. Conjugate natural convection with conduction

Now, we focus our attention on the conjugate natural convection/conduction problem to investigate the conduction effect of solid body on the heat transfer characteristics across the cavity. When the Rayleigh number is low, $Ra = 10^3$, as shown in Fig. 7, the existence of a conducting body reduced the convection, with the maximum value of absolute streamfunction decreasing to $|\psi|_{\max} = 0.237$ from $|\psi|_{\max} = 1.17$ in Fig. 3, and so, conduction played a fully dominant role in the process of heat transfer. Further, since the solid body with a high relative thermal conductivity of $k^* = 5$, the averaged Nusselt number increased to $\overline{Nu} = 1.418$, approximately 30% higher than that of the pure convection case. As expected, the heatlines basically follow the principle of heat conduction, exhibiting a group of parallel lines. It is worth noting that the heat flux lines in the solid conducting body are consistent with the heatlines as explained before.

Fig. 8 presents the results for $Ra = 10^4$. The convection is largely weakened by the inserted solid body. However, the solid body directly conducts heat from the hot fluid in the top-left part to the cold fluid in the bottom-right part, which acts like "short circuiting". The conduction of solid body reduced the temperature difference between the hot and cold fluid, and eventually substantially degraded the strength of convection as compared to the pure natural convection case at $Ra = 10^4$ shown in Fig. 6, decreased from previous $|\psi|_{\max} = 5.04$ to present $|\psi|_{\max} = 1.98$. As a result, the total heat transfer across the cavity, as represented by the average Nusselt number or maximum heatline value, is decreased to $\overline{Nu} = 1.794$, 20% lower than that in Fig. 4.

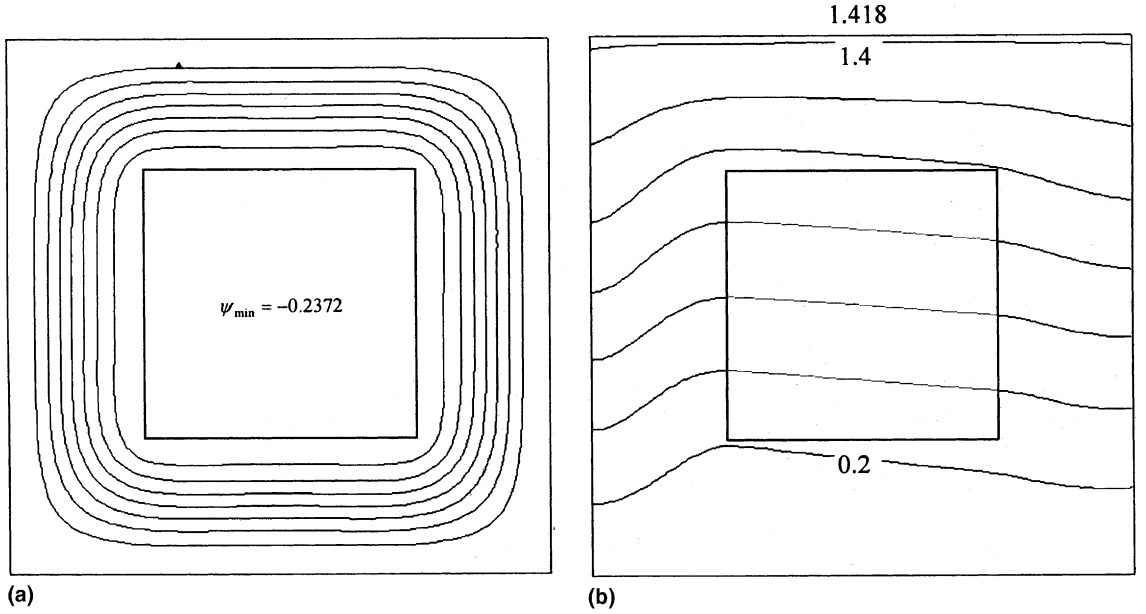

Fig. 7. Results of conjugate natural convection at $Ra = 10^3$ in an air-filled square cavity with a conducting body of $k^* = 5$: (a) Streamlines whose incremental step is 0.03; (b) heatlines whose incremental step is 0.2.

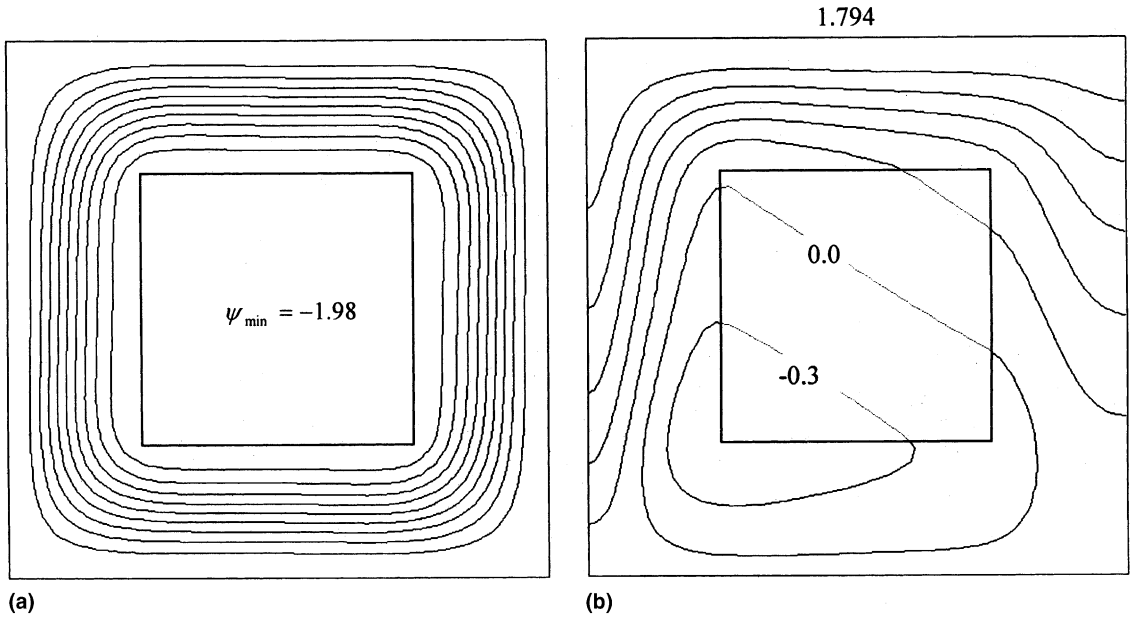

Fig. 8. Results of conjugate natural convection at $Ra = 10^4$ in an air-filled square cavity with a conducting body of $k^* = 5$: (a) Streamlines whose incremental step is 0.2; (b) heatlines whose incremental step is 0.3.

As Rayleigh number increased further up to 10^5, depicted in Fig. 9, however, things are different: there are only slight variations between the conjugate and the pure convection cases, with the convection strength and the average Nusselt number, respectively, decreasing from the former value of $|\psi|_{max} = 9.50$ and $\overline{Nu} = 4.557$ in Fig. 5 to present $|\psi|_{max} = 8.41$ and $\overline{Nu} = 4.372$. The convection now becomes a dominant mode in the process of heat transfer. The rarity of heatlines through the solid body reveals that the amount of heat transported

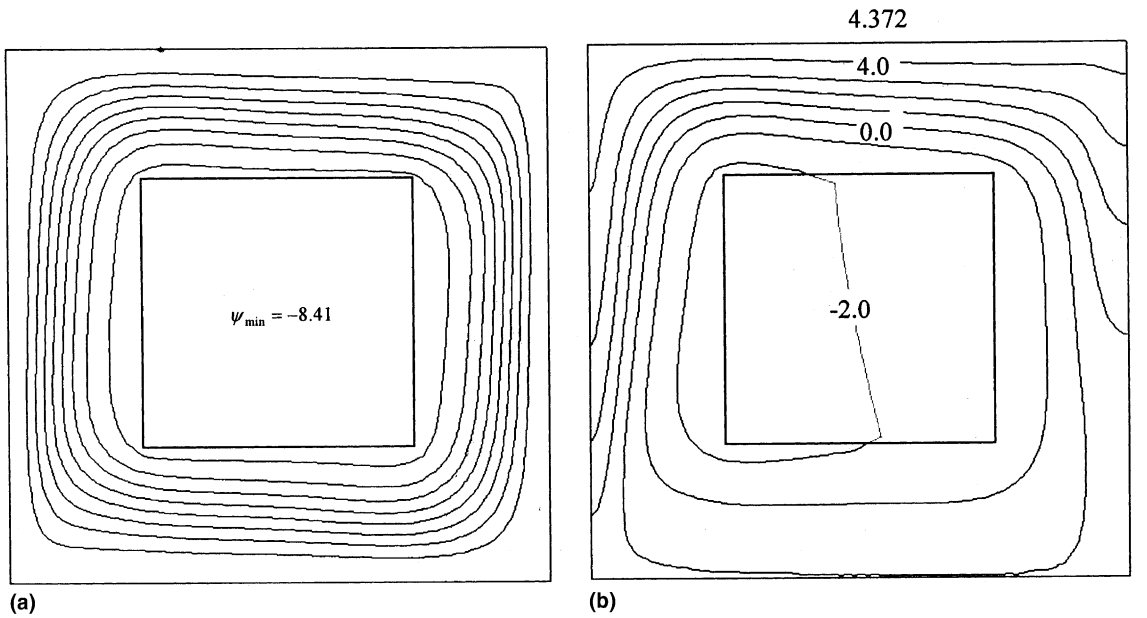

Fig. 9. Results of conjugate natural convection at $Ra = 10^5$ in an air-filled square cavity with a conducting body of $k^* = 5$: (a) Streamlines whose incremental step is 1.0; (b) heatlines whose incremental step is 1.0.

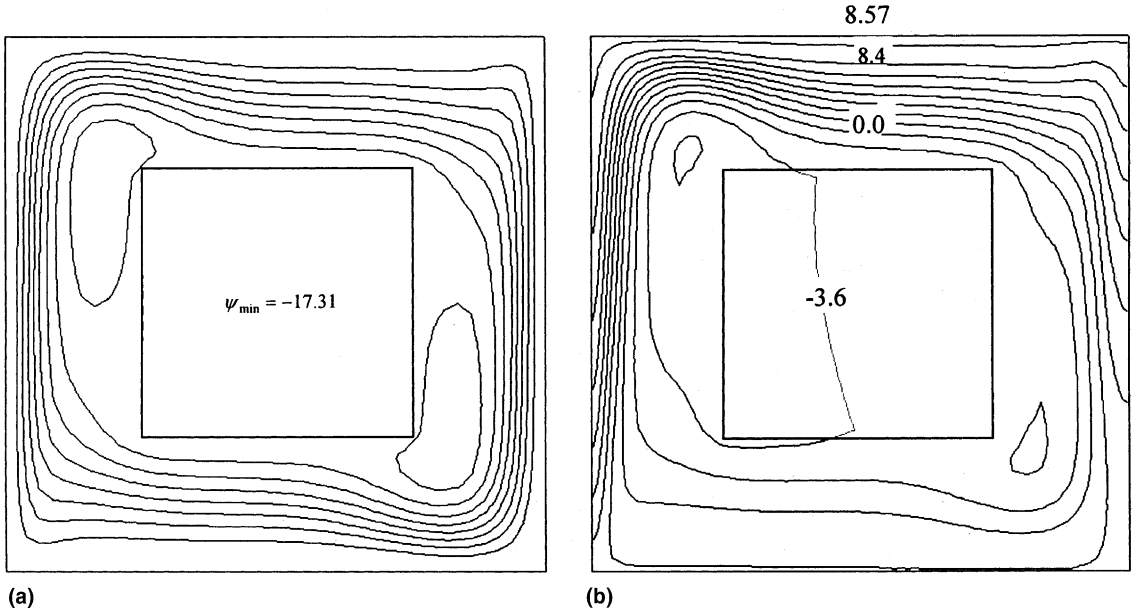

Fig. 10. Results of conjugate natural convection at $Ra = 10^6$ in an air-filled square cavity with a conducting body of $k^* = 5$: (a) Streamlines whose incremental step is 2.0; (b) heatlines whose incremental step is 1.2.

by the conduction is tiny. The solid body of $k^* = 5$ would enhance the conduction to a certain extent, and accordingly reduced the convection, which results in lower heat transfer.

Results for $Ra = 10^6$ are presented in Fig. 10. The same trend as the case $Ra = 10^5$ occurs. The presence of solid body is beneficial to the rapidly growing convection and impels it moving outward, and thus two vortices appear at the corner of the solid body, which results in increasing the convection to some extent.

4. Conclusions

In this paper, the method of using functions and lines to visualize the momentum and heat transport for convective heat transfer has been detailed analyzed. It was used to exhibit the inherent structures or characteristics of heat and fluid flow for natural convection and conjugate natural convection/heat conduction. The following conclusions can be obtained:

1. The functions defined based on dimensionless variables are more general and straightforward than that in dimensional form.
2. The basic characteristics of functions/lines, are useful for perceiving the visualization results.
3. The functions and lines are unified for both fluid and solid regions when dealing with conjugate problem. It is not needed to calculate the coefficients of heatfunction at the fluid–solid interface, and meanwhile, heatfunction values at the fluid–solid interface are not needed any more for drawing heatlines, which make it easier to handle conjugate heat transfer problem.
4. Visualization results by streamlines and heatlines directly exhibit the nature of fluid flow and heat transfer in macroscopical level, and hence, provides a more vigorous means to discuss the convective heat transfer accordingly.

References

[1] S. Kimura, A. Bejan, The 'heatline' visualization of convective heat transfer, ASME J. Heat Transfer 105 (1983) 916–919.
[2] D. Littlefield, P. Desai, Buoyant laminar convection in a vertical cylindrical annulus, ASME J. Heat Transfer 108 (1986) 814–821.
[3] F.L. Bello-Ochende, A heat function formulation for thermal convection in a square cavity, Comput. Methods Appl. Mech. Eng. 68 (1988) 141–149.
[4] S.K. Aggarwal, A. Manhapra, Use of heatlines for unsteady buoyancy-driven flow in a cylindrical enclosure, ASME J. Heat Transfer 111 (1989) 576–578.
[5] C.J. Ho, Y.H. Lin, Natural convection of cold water in a vertical annulus with constant heat flux on the inner wall, ASME J. Heat Transfer 112 (1990) 117–123.
[6] Al.M. Morega, A. Bejan, Heatline visualization of forced convection boundary layers, Int. J. Heat Mass Transfer 36 (1993) 3957–3966.
[7] H.Y. Wang, F. Penot, J.B. Sauliner, Numerical study of a buoyancy-induced flow along a vertical plate with

discretely heated integrated circuit packages, Int. J. Heat Mass Transfer 40 (1997) 1509–1520.
[8] V.A.F. Costa, Double diffusive natural convection in a square enclosure with heat and mass diffusive walls, Int. J. Heat Mass Transfer 40 (1997) 4061–4071.
[9] V.A.F. Costa, Unification of the streamline, heatline and massline methods for the visualization of two-dimensional transport phenomena, Int. J. Heat Mass Transfer 42 (1999) 27–33.
[10] S.V. Patankar, Numerical Heat Transfer and Fluid Flow, Hemisphere, Washington, DC, 1980.
[11] S. Thakur, W. Shyy, Some implementational issues of convection schemes for finite-volume formulations, Numer. Heat Transfer, Part B 24 (1993) 31–55.
[12] G. Vahl Davis, Natural convection of air in a square cavity: a bench mark numerical solution, Int. J. Numer. Methods Fluids 3 (1983) 249–263.